

EPIC247098361b: a transiting warm Saturn on an eccentric $P = 11.2$ days orbit around a $V = 9.9$ star

R. Brahm,^{1,2*} N. Espinoza,^{3,8} A. Jordán,^{2,1,3} F. Rojas,² P. Sarkis,³ M. R. Díaz,⁴ M. Rabus,^{2,3} H. Drass,^{1,5} R. Lachaume,^{2,3} M. G. Soto,⁴ J. S. Jenkins,⁴ M. I. Jones,⁶ Th. Henning,³ B. Pantoja,⁴ M. Vučković,⁷

¹Millennium Institute of Astrophysics, Santiago, Chile

²Instituto de Astrofísica, Facultad de Física, Pontificia Universidad Católica de Chile, Av. Vicuña Mackenna 4860, 7820436 Macul, Santiago, Chile

³Max-Planck-Institut für Astronomie, Königstuhl 17, 69117 Heidelberg, Germany

⁴Departamento de Astronomía, Universidad de Chile, Camino El Observatorio 1515, Las Condes, Santiago, Chile

⁵Center of Astro-Engineering UC, Pontificia Universidad Católica de Chile, Av. Vicuña Mackenna 4860, 7820436 Macul, Santiago, Chile

⁶European Southern Observatory, Casilla 19001, Santiago, Chile

⁷Instituto de Física y Astronomía, Universidad de Valparaíso, Casilla 5030, Valparaíso, Chile

⁸Bernoulli Fellow

Draft Version 4.0

ABSTRACT

We report the discovery of EPIC247098361b using photometric data of the Kepler K2 satellite coupled with ground-based spectroscopic observations. EPIC247098361b has a mass of $M_P = 0.397 \pm 0.037 M_J$, a radius of $R_P = 1.00 \pm 0.020 R_J$, and a moderately low equilibrium temperature of $T_{eq} = 1030 \pm 15$ K due to its relatively large star-planet separation of $a = 0.1036$ AU. EPIC247098361b orbits its bright ($V = 9.9$) late F-type host star in an eccentric orbit ($e = 0.258 \pm 0.025$) every 11.2 days, and is one of only four well characterized warm Jupiters having hosts stars brighter than $V = 10$. We estimate a heavy element content of $20 \pm 7 M_{\oplus}$ for EPIC247098361b, which is consistent with standard models of giant planet formation. The bright host star of EPIC247098361b makes this system a well suited target for detailed follow-up observations that will aid in the study of the atmospheres and orbital evolution of giant planets at moderate separations from their host stars.

Key words:

1 INTRODUCTION

Transiting hot Jupiters (giant planets with periods $P < 10$ d) have been efficiently detected by several ground- and space-based surveys (e.g., Bakos et al. 2004; Pollacco et al. 2006; Borucki et al. 2010; Bakos et al. 2013). This great number of discoveries has been key for constraining theories of their formation, structure and evolution (for a recent review see Dawson & Johnson 2018), but several unsolved theoretical challenges have emerged from these observations as well. For example, the specific source of the inflated radius of highly irradiated hot Jupiters is a topic of active research. While several mechanisms have been proposed (for a review see Spiegel & Burrows 2012), their validation is not straightforward because in most cases the structural composition (i.e.

heavy element content) of these planets is not known, and therefore the problem becomes degenerate.

Another long standing theoretical challenge is the actual existence of these massive planets at short orbital separations, because most theoretical models of formation require that Jovian planets are formed beyond the snow line where solid embryos are efficiently accreted (Rafikov 2006). While some orbital displacement of the planet due to exchange of angular momentum with a gaseous protoplanetary disc is expected to happen, it is not clear that this type of interaction can account for the currently known population of giant planets with semi-major axes shorter than 1 AU. One particular challenge is that a significant fraction of the hot Jupiter systems have been found to have large spin-orbit angles, which are not expected to arise in a gentle disc migration scenario (for a review see Winn & Fabrycky 2015). While high eccentricity migration models predict the existence of highly misaligned spin-orbit an-

* E-mail: rbrahm@astro.puc.cl

gles, a direct comparison between the model predictions and the obliquity distribution of hot Jupiters can be affected by the possible realignment of the outer layers of the star due to tidal and/or magnetic interactions (Dawson 2014; Li & Winn 2016).

Transiting warm Jupiters (giant planets with periods $P > 10$ d) are valuable systems in the above mentioned context. Due to their relatively long planet-star separations ($a \gtrsim 0.1$ AU), the internal structure of warm Jupiters is not significantly affected by the tidal, magnetic and/or radiative mechanisms that can significantly affect hot Jupiters. For this reason, theoretical models can be used to investigate the internal composition of giant planets and how this depends on the global properties of the system (i.e., stellar mass, [Fe/H], multiplicity) in a more straightforward fashion. Along the same line, given that for warm Jupiters the planet-star interaction is in general not strong enough to realign the outer layers of the star, they are better suited systems to test the predictions of high eccentricity migration models by studying the distribution of spin-orbit angles (Petrovich & Tremaine 2016).

Unfortunately, the detection of warm Jupiters around bright stars is hindered by strong detection biases. The transit probability is proportional to a^{-1} , and additionally the duty cycle required to discover transiting planets with periods longer than 10 days is usually too high for typical ground-based surveys, which are the ones that have made the most significant contribution to the population of transiting giant planets with precisely determined masses and radii. One workaround to this problem is to build longitudinal networks of identical telescopes to counteract the diurnal cycle (e.g. HATSouth, Bakos et al. 2013). This configuration has allowed the detection of planets with periods as long as 16 days (Brahm et al. 2016b). Another solution is the use of space-based telescopes. Due to the precise and continuous ≈ 2 month observations per field, the Kepler K2 mission (Howell et al. 2014) is able to detect warm Jupiters (Smith et al. 2017; Shporer et al. 2017). Additionally, it has an increased probability of detecting these type of system on bright stars compared to the original *Kepler* mission because it surveys a larger area of the sky.

In this study we present the discovery of a warm Saturn around a bright star with the *Kepler* telescope. This discovery was performed in the context of the K2CL collaboration, which uses spectroscopic facilities located in Chile to confirm and characterize transiting planets from K2 (Brahm et al. 2016a; Espinoza et al. 2017a; Jones et al. 2017; Soto et al. 2018). The structure of the paper is as follows. In § 2 we present the photometric and spectroscopic observations that allowed the discovery of EPIC247098361b, in § 3 we derive the planetary and stellar parameters, and we discuss our findings in § 4.

2 OBSERVATIONS

2.1 Kepler K2

EPIC247098361 was observed by the Kepler K2 mission between March and May 2017, while carrying out the monitoring for campaign 13. The photometric data was reduced from pixel-level products using the EVEREST algorithm

(Luger et al. 2016, 2017). Long-term trends in the data are corrected with a gaussian-process regression. Transiting planet detection is performed by using the Box-fitting Least Squares algorithm (Kovács et al. 2002) on the processed light curves. With this procedure we identified a 11.17 day periodic signal, with a depth consistent with that of a giant planet transiting a main sequence star. The (detrended) K2 photometry for this target star is shown in Figure 1. Due to the clear box-shaped transits and the brightness of the star, EPIC247098361 was selected as a high priority target for spectroscopic follow-up observations.

2.2 Spectroscopic Observation

High resolution spectroscopic observations are required to characterize the host star, identify possible false positive scenarios, and to confirm the planetary nature of the transiting companion via mass determination from the radial velocity signal. The spectroscopic facilities that were used in this work are summarized in Table 1, along with the main properties of the observations.

We obtained three spectra of EPIC247098361 with the Coralie spectrograph (Queloz et al. 2001) mounted on the 1.2m Euler/Swiss telescope located at the ESO La Silla observatory. Observations were obtained on three consecutive nights in October 2017, and they were acquired with the simultaneous calibration mode (Baranne et al. 1996) where a secondary fiber is illuminated by a Fabry-Perot etalon in order to trace the instrumental velocity drift produced by the changes in the environmental conditions of the instrument enclosure. Coralie data was processed and analyzed with the CERES automated package (Jordán et al. 2014; Brahm et al. 2017a). On top of the reduction and optimal extraction of the spectra, CERES delivers precision radial velocity and bisector span measurements by using the cross-correlation technique, and an initial estimate of the atmospheric parameters by comparing the reduced spectra with a grid of synthetic models (Coelho et al. 2005). These three spectra allowed us to conclude that EPIC247098361 is a dwarf star ($\log(g) \approx 4.2$) with an effective temperature of $T_{eff} \approx 5900$ K. Additionally, there was no evidence of additional stellar components in the spectra that could be linked to blended eclipsing binary scenarios, and the radial velocity measurements rejected the presence of large velocity variations caused by a stellar mass orbital companion. These properties boosted the follow-up observations of EPIC247098361 and we proceeded to obtain spectra with more powerful facilities.

We obtained 18 spectra of EPIC247098361 between October of 2017 and January 2018 with the FEROS spectrograph (Kaufer et al. 1999) mounted on the MPG2.2m telescope, and another eight spectra of the same target in November 2017 with the HARPS spectrograph (Mayor et al. 2003) mounted on the ESO 3.6m telescope. Both facilities are located at the ESO La Silla Observatory. The FEROS observations were performed with the simultaneous calibration mode where a Thorium-Argon lamp illuminates a second fiber during the science observations. Given that the nightly instrumental drift of the HARPS spectrograph is significantly smaller than the expected radial velocity variation produced by a giant planet, the secondary fiber of this instrument was not used to trace the velocity drift. Re-

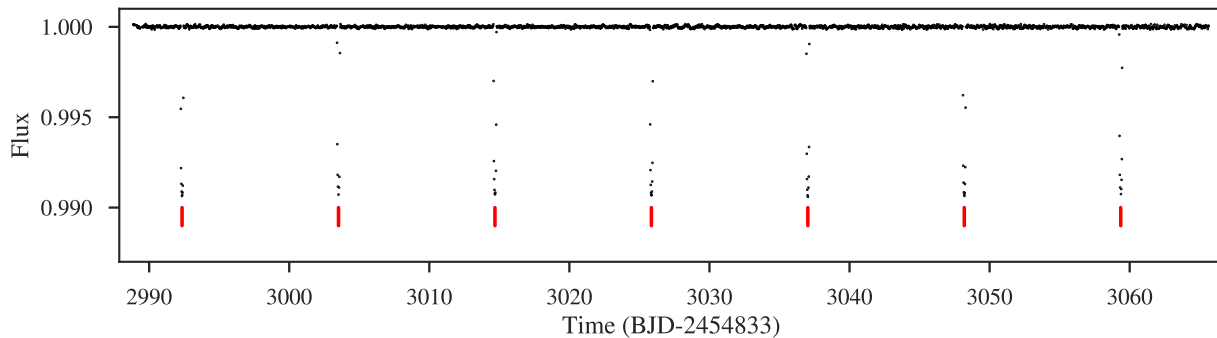


Figure 1. Detrended K2 photometry of EPIC 247098361. The transits of our planet candidate have been identified by red marks below each event.

Table 1. Summary of spectroscopic observations for EPIC247098361.

Instrument	UT Date(s)	N Spec.	Resolution	S/N range	γ_{RV} [km s ⁻¹]	RV Precision [m s ⁻¹]
Coralie / 1.2m Euler/Swiss	2017 Oct 31 – Nov 2	3	60000	27 – 44	22.327	10
FEROS / 2.2m MPG	2017 Oct 03 – 2018 Jan 28	18	50000	106 – 167	22.398	7
HARPS / 3.6m ESO	2017 Nov 01 – 2017 Nov 08	8	115000	36 – 50	22.416	6

ductions and analysis of FEROS and HARPS spectra were performed with the CERES automated package. The radial velocity and bisector span measurements are presented in Table 4, and the radial velocity curve is plotted in Figure 2. As can be seen in this figure, the velocities obtained with the three instruments are consistent with the radial velocity variation produced by a giant planet with an eccentric orbit. Additionally, no significant correlation was detected between the radial velocities and bisector span measurements, as can be seen in the radial velocity vs. bisector span (BIS) scatter plot on Figure 3. We computed the distribution for the Pearson correlation coefficient between the radial velocities and bisector span measurements, finding that it lies between -0.13 and 0.65 at 95% confidence level, and is therefore consistent with no correlation. These spectroscopic observations allowed us to confirm that the transit-like signal observed in the K2 data is produced by a planetary mass companion.

3 ANALYSIS

3.1 Stellar parameters

We used the co-added FEROS spectra to estimate the stellar atmospheric parameters of EPIC247098361 by using the ZASPE code (Brahm et al. 2015, 2017b). ZASPE determines T_{eff} , $\log(g)$, $[Fe/H]$, and $v\sin(i)$ by comparing the observed spectra to synthetic ones in the spectral regions most sensitive to changes in those parameters. Additionally, reliable uncertainties are obtained from the data by performing Monte Carlo simulations that take into account the systematic mismatches between data and models. Using this procedure we obtain the following parameters: $T_{eff} = 6020 \pm 83$ K, $\log(g) = 4.22$ dex, $[Fe/H] = 0.04$ dex, and $v\sin(i) = 4.0$ km s⁻¹, which are consistent with the initial estimates provided by CERES.

EPIC247098361 was observed by GAIA and its parallax is given on its DR1 ($p = 7.69 \pm 0.27$ mas, Gaia Collabora-

tion et al. 2016a,b). We used this parallax value coupled to the reported magnitudes in different bandpass to estimate the stellar radius, following an approach similar to Barragán et al. (2017). Specifically, we used the BT-Settl-CIFIST spectral models from Baraffe et al. (2015), interpolated in T_{eff} and $\log(g)$, to generate a synthetic spectral energy distribution (SED) consistent with the atmospheric parameters of EPIC247098361. We then integrated the SED in different spectral regions to generate synthetic magnitudes that were weighted by the corresponding transmission functions of the passband filters. The synthetic SED along with the observed flux density in the different filters are plotted in Figure 4.

These synthetic magnitudes were used to infer the stellar radius (R_*) and the extinction factor (A_V) by comparing them to the observed magnitudes after applying a correction of the dilution of the stellar flux due to the distance. Specifically, our data was the stellar luminosity obtained by multiplying the observed flux density $F_{obs}^{\lambda_i}$ at the different passband filters (λ_i) with the square of the distance inferred from the GAIA parallax (D):

$$L_{obs} = 4\pi F_{obs}^{\lambda_i} D^2. \quad (1)$$

While the adopted model was:

$$L_{mod} = 4\pi F_{syn}^{\lambda_i} R_*^2 e^{-A(\lambda_i)/2.5}, \quad (2)$$

where $F_{syn}^{\lambda_i}$ is the synthetic flux density at the different passband filters, and $A(\lambda_i)$ is the wavelength dependent extinction factor, which we take to be a function of visual extinction (A_V) as described in Cardelli et al. (1989). We used the emcee Python package (Foreman-Mackey et al. 2013) to sample the posterior distribution of R_* and A_V . Figure 5 shows the posterior distribution for the parameters. The estimated stellar radius from the parallax measurement was coupled to the estimated T_{eff} to obtain the mass and evolutionary stage of the star by using the Yonsei-Yale isochrones (Yi et al. 2001). Figure 6 shows the isochrones in the T_{eff} - R_* plane for different ages, with the values for EPIC247098361 indicated with a blue cross. This analysis allowed us to ob-

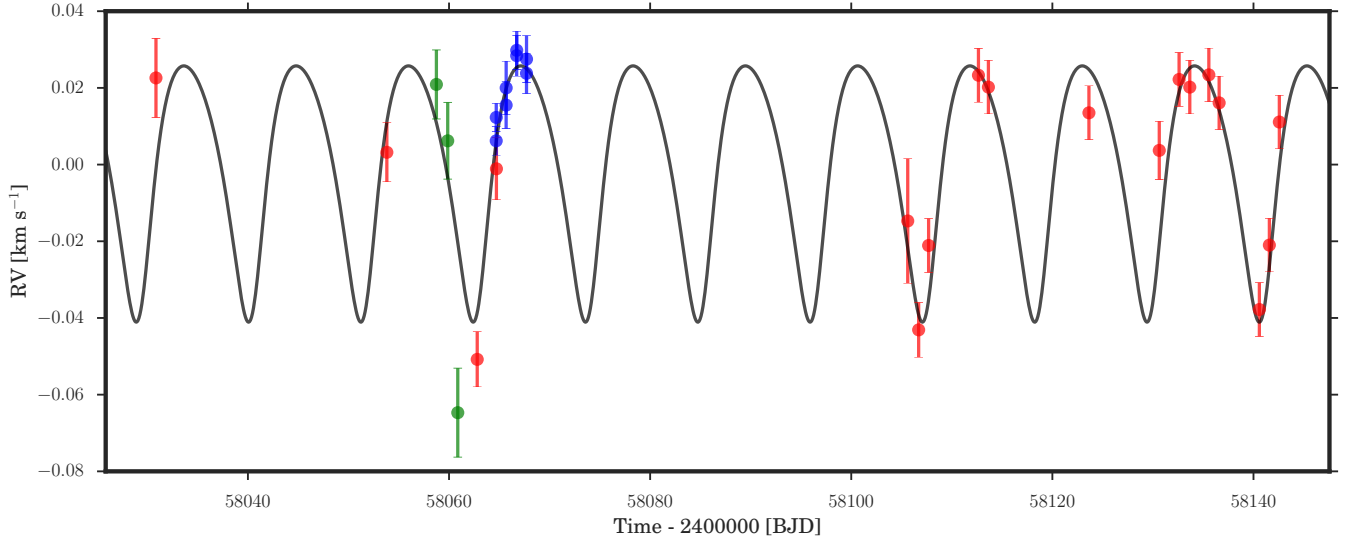


Figure 2. Radial velocity (RV) curve obtained with FEROS (red), Coralie (green) and HARPS (blue). The black line corresponds to the Keplerian model with the posterior parameters found in Section 3.

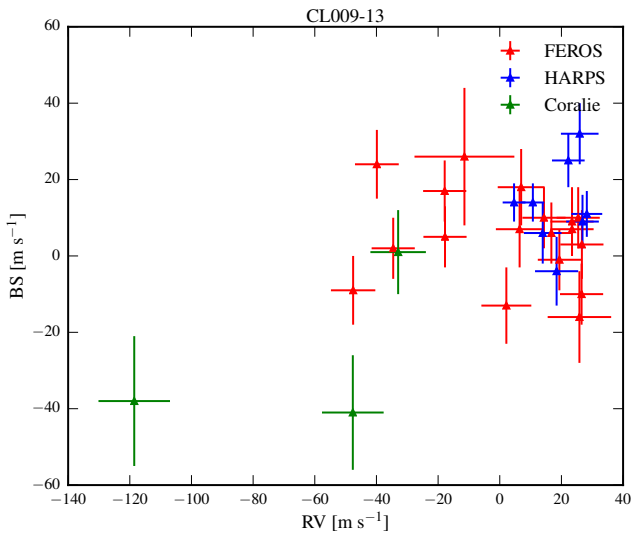


Figure 3. Radial velocity (RV) versus bisector span (BS) scatter plot using data from our spectroscopic observations of EPIC247098361. No significant correlation was found.

tain a more precise estimate for the stellar $\log(g)$ than the value obtained with ZASPE. This new $\log(g)$ value was held fixed in a new ZASPE iteration, which was followed by a new estimate of the stellar radius and a new comparison with the theoretical isochrones. After this final iteration, the stellar $\log(g)$ value converged to 4.389 ± 0.017 , and the other stellar properties to the values listed in Table 2. We found that EPIC247098361 is a late F-dwarf star ($M_* = 1.192 \pm 0.025 M_\odot$, $R_* = 1.161 \pm 0.022 R_\odot$) and that it is slightly metal rich ($[\text{Fe}/\text{H}] = 0.1 \pm 0.04$).

Table 2. Stellar properties and parameters for EPIC247098361.

Parameter	Value	Method / Source
Names	EPIC247098361	–
RA	04:55:03.96	–
DEC	18:39:16.33	–
Parallax [mas]	7.69 ± 0.27	GAIA
K_p (mag)	9.789	EPIC
B (mag)	10.469 ± 0.029	APASS
g (mag)	10.286 ± 0.184	APASS
V (mag)	9.899 ± 0.039	APASS
r (mag)	9.749 ± 0.033	APASS
i (mag)	9.663 ± 0.011	APASS
J (mag)	8.739 ± 0.025	2MASS
H (mag)	8.480 ± 0.011	2MASS
Ks (mag)	8.434 ± 0.014	2MASS
W1 (mag)	8.380 ± 0.024	WISE
W2 (mag)	8.419 ± 0.019	WISE
W3 (mag)	8.391 ± 0.027	WISE
T_{eff} [K]	6154 ± 60	ZASPE
$\log(g)$ [dex]	4.379 ± 0.017	ZASPE
$[\text{Fe}/\text{H}]$ [dex]	0.10 ± 0.04	ZASPE
$v \sin i$ [km s^{-1}]	4.16 ± 0.282	ZASPE
M_* [M_\odot]	$1.192^{+0.025}_{-0.024}$	ZASPE + GAIA + YY
R_* [R_\odot]	$1.161^{+0.023}_{-0.021}$	ZASPE + GAIA
L_* [L_\odot]	$1.718^{+0.101}_{-0.086}$	ZASPE + GAIA + YY
Age [Gyr]	$1.26^{+0.71}_{-0.74}$	ZASPE + GAIA + YY
A_V	$0.129^{+0.065}_{-0.062}$	ZASPE + GAIA

3.2 Global modelling

We performed a joint analysis of the *Kepler* K2 data and follow-up radial velocities in order to determine the transit and orbital parameters of the planetary system. For this purpose we used the `exonailer` code which is described in detail in Espinoza et al. (2016). Briefly, we model the tran-

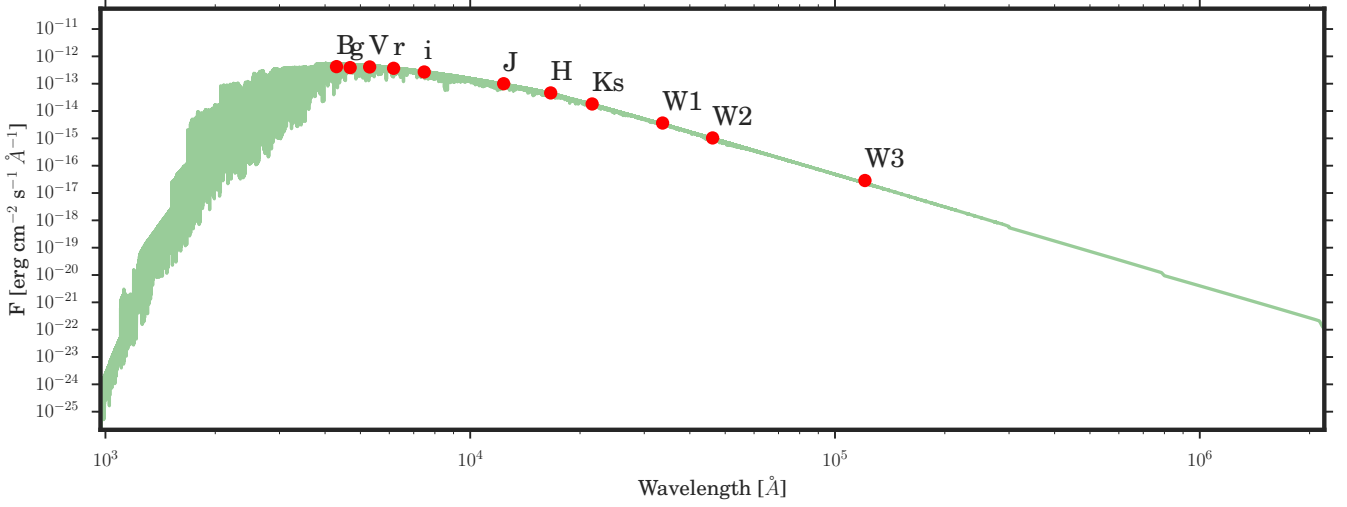


Figure 4. Spectral energy distribution of the BT-Settl-CIFIST model with atmospheric parameters similar to EPIC247098361. The observed flux densities for the different passband filters are identified as red circles.

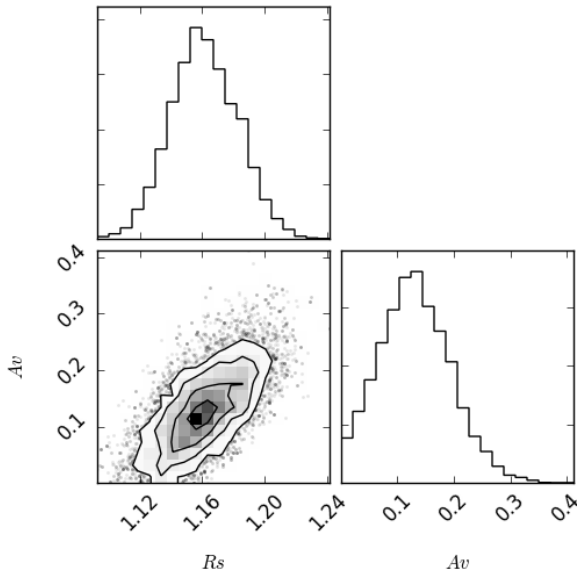


Figure 5. Triangle plot for the posterior distributions of R_* and A_V obtained from the observed magnitudes and GAIA parallax.

sit light curves using the `batman` package (Kreidberg 2015) and we fit them with the resampling method described in Kipping (2013a) in order to account for the smearing effect of the K2 long-cadence light curves. Following the results of Espinoza & Jordán (2015), we fit for the limb-darkening coefficients simultaneously with the other transit parameters, and followed Espinoza & Jordán (2016) to select the quadratic limb-darkening as the optimal law to use for the case of EPIC247098361, as this law provides the lowest expected mean-squared error in the planet-to-star radius ratio. The limb-darkening coefficients were fit using the uninformative sampling technique of Kipping (2013b). A photometric

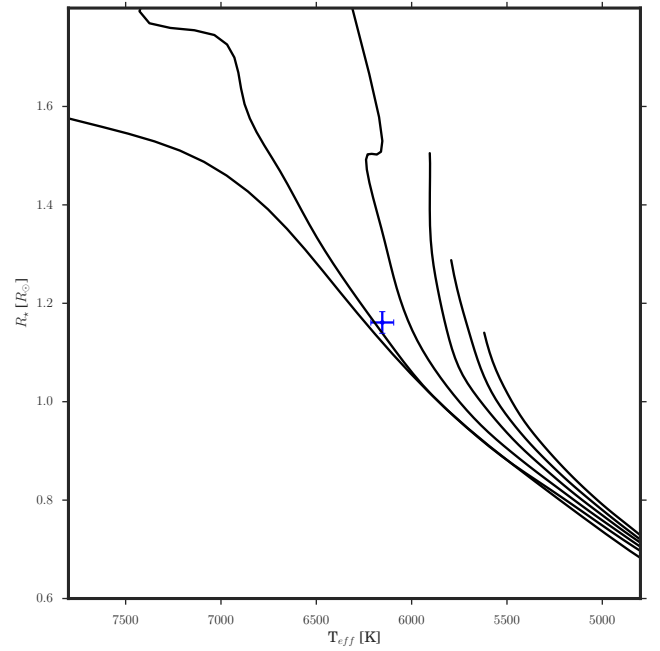


Figure 6. Yonsei-Yale isochrones for the metallicity of EPIC247098361 in the T_{eff} - R_* plane. From left to right the isochrones corresponds to 0.1, 1, 3, 5, 7, 9 Gyr. The position of EPIC247098361 in this plane is shown with a blue cross.

jitter term was also included in the fit of the photometry, in order to empirically estimate the noise of the light curves. The radial velocities are modelled with the `rad-vel` package (Fulton et al. 2018), where we consider a different systemic velocity and jitter factor for each instrument. Additionally, we consider the eccentricity and argument of periastron passage as free parameters with uniform priors (an eccentric fit to the whole dataset is preferred to a circular model with a $\Delta\text{BIC} = 14$ in favor of the eccentric fit), and put a prior on

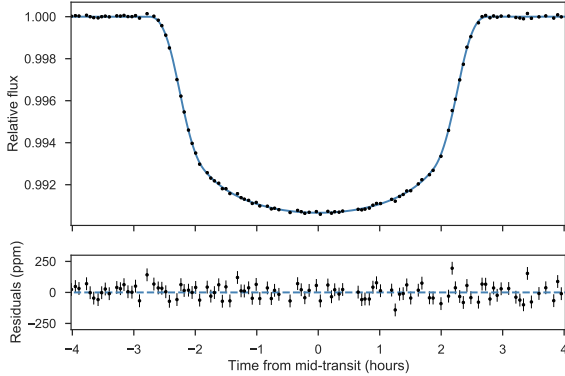


Figure 7. The top panel shows the phase folded Kepler *K2* photometry (black points) as a function of time at the time of transit for EPIC247098361b, and the model constructed with the derived parameters of exonailer (blue line). The bottom panel shows the corresponding residuals.

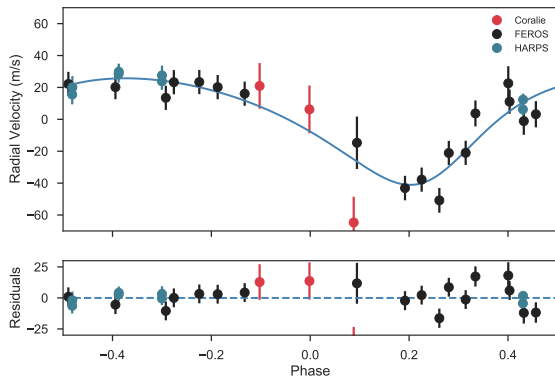


Figure 8. The top panel presents the radial velocities (colored circles) obtained with the three spectrographs as a function of the orbital phase. The RV model with the derived orbital parameters for EPIC247098361b is also plotted (blue line). The bottom panel shows the residuals obtained for these radial velocity measurements.

a/R_* using the value obtained by our procedures described in § 3.1, which gave $a/R_* = 19.30 \pm 0.35$, a more precise value than the one obtainable from the transit light curve alone. The priors and posteriors of our modelling are listed in Table 3. The transit and radial velocity models generated from the posterior distribution are presented in Figures 7 and 8, along with the observed data. We used these transit and orbital parameters to obtain the physical parameters of the planet by using the stellar properties obtained in the previous subsections. We found that EPIC247098361b has a Saturn-like mass of $M_P = 0.397 \pm 0.037 M_J$, a Jupiter-like radius of $R_P = 1.000 \pm 0.020 R_J$, and an equilibrium temperature of $T_{eq} = 991 \pm 12$ K. Additionally we found that the planet has a significantly eccentric orbit of $e = 0.258 \pm 0.025$.

3.3 Rotational modulation and search of additional transits

A search for additional transits was performed on the photometry using the BLS algorithm (Kovács et al. 2002) with the transits of EPIC 247098361b masked out. No significant signals were found, which puts a limit of $\approx 1.5R_{\oplus}$ to any transiting companion orbiting in periods smaller than ≈ 38 days. Additionally, a Generalized Lomb-Scargle periodogram (Zechmeister & Kürster 2009) was ran in order to search for any periodic signals in the data, but the only periods that stood out were at 1.04 and 0.74 days, most likely instrumental as the phased data at those periods does not show any significant, physically interpretable signal. No secondary eclipses or phase curve modulations were found in the data, which is expected given that the secondary eclipse amplitude due to reflected light would be at most $(R_p/a)^2 = 21 \pm 0.71$ ppm, significantly below the photometric precision of 51 ppm.

4 DISCUSSION

EPIC247098361b is compared with the full population of transiting planets with available determinations of radii and masses at the level of 20% in Figures 9 and 10. Due to its orbital period of $P = 11.2$ d, EPIC247098361b lies in a relatively sparsely populated region of parameter space. Its time averaged equilibrium temperature of 1030 K lies just in the transition region where the mechanism responsible for inflating the radii of hot Jupiters stops playing a significant role (Kovács et al. 2010; Demory & Seager 2011). Additionally, its current planet-to-star separation at pericenter is large enough that the effects that tidal and/or magnetic interactions can have on the structure and orbital evolution of the system are expected to be small (Dawson 2014).

EPIC247098361b is remarkably similar to WASP-117b (Lendl et al. 2014). Both have Saturn-like masses, Jupiter-like radii, eccentricities close to 0.3, orbital periods slightly longer than 10 days, and late F-type host stars. WASP-117b has a slightly less metal rich host star than EPIC247098361 and its density is lower. Both systems are excellent targets for performing detailed follow-up observations to further understand the structure and evolution of giant planets that are not affected by proximity effects. According to TEPICat (Southworth 2011), there are only ≈ 20 other well characterised transiting giant planets with periods longer than 10 days. EPIC247098361b ($V = 9.9$) stands out as the system with the brightest host star after HD 17156 ($V = 8.2$, Barbieri et al. 2007) and HD 80606 ($V = 9.1$, Moutou et al. 2009).

4.1 Structure

Due to the moderately low insolation levels received from its parent star, the internal structure of EPIC247098361b can be studied by comparing its measurements of mass and radius with the predictions of theoretical models. We used the (Fortney et al. 2007) models of planetary structure and evolution to determine the mass of a possible central rocky core. These simple models assume that all the solid material is concentrated in this core, which is likely a simplification

Table 3. Transit, orbital, and physical parameters of EPIC247098361b. On the priors, $N(\mu, \sigma)$ stands for a normal distribution with mean μ and standard deviation σ , $U(a, b)$ stands for a uniform distribution between a and b , and $J(a, b)$ stands for a Jeffrey’s prior defined between a and b .

Parameter	Prior	Value
Light-curve parameters		
P (days)	$N(11.169, 0.1)$	11.168454 ± 0.000023
T_0 (days)	$N(2457825.350, 0.1)$	$2457825.3497822732 \pm 0.000093$
R_P/R_\star	$U(0.001, 0.2)$	$0.08868^{+0.00044}_{-0.00042}$
a/R_\star	$N(19.30, 0.35)$	$19.25^{+0.27}_{-0.31}$
i	$U(70, 90)$	$89.14^{+0.13}_{-0.11}$
q_1	$U(0, 1)$	$0.417^{+0.038}_{-0.037}$
q_2	$U(0, 1)$	$0.318^{+0.029}_{-0.028}$
σ_w (ppm)	$J(10, 5000)$	$51.68^{+0.68}_{-0.64}$
RV parameters		
K (m s^{-1})	$N(35, 100)$	$33.42^{+3.12}_{-3.02}$
e	$U(0, 1)$	0.258 ± 0.025
ω (deg)	$U(0, 360)$	$207^{+3.6}_{-3.8}$
$\gamma_{coralie}$ (km s^{-1})	$N(22.35, 0.05)$	$22.3394^{+0.0087}_{-0.0092}$
γ_{feros} (km s^{-1})	$N(22.40, 0.05)$	$22.3965^{+0.0023}_{-0.0022}$
γ_{harpis} (km s^{-1})	$N(22.40, 0.05)$	$22.3917^{+0.0029}_{-0.0030}$
$\sigma_{coralie}$ (km s^{-1})	$J(10^{-4}, 0.1)$	$0.0011^{+0.0013}_{-0.0010}$
σ_{feros} (km s^{-1})	$J(10^{-4}, 0.1)$	$0.0029^{+0.0042}_{-0.0025}$
σ_{harpis} (km s^{-1})	$J(10^{-4}, 0.1)$	$0.0008^{+0.0024}_{-0.0006}$
Derived parameters		
M_P (M_J)	–	0.397 ± 0.037
R_P (R_J)	–	$1.000^{+0.019}_{-0.020}$
$\langle T_{eq} \rangle^a$ (K)	–	1030 ± 15
a (AU)	–	$0.10355^{+0.00078}_{-0.00076}$

*Time averaged equilibrium temperature using equation 16 of Méndez & Rivera-Valentín (2017).

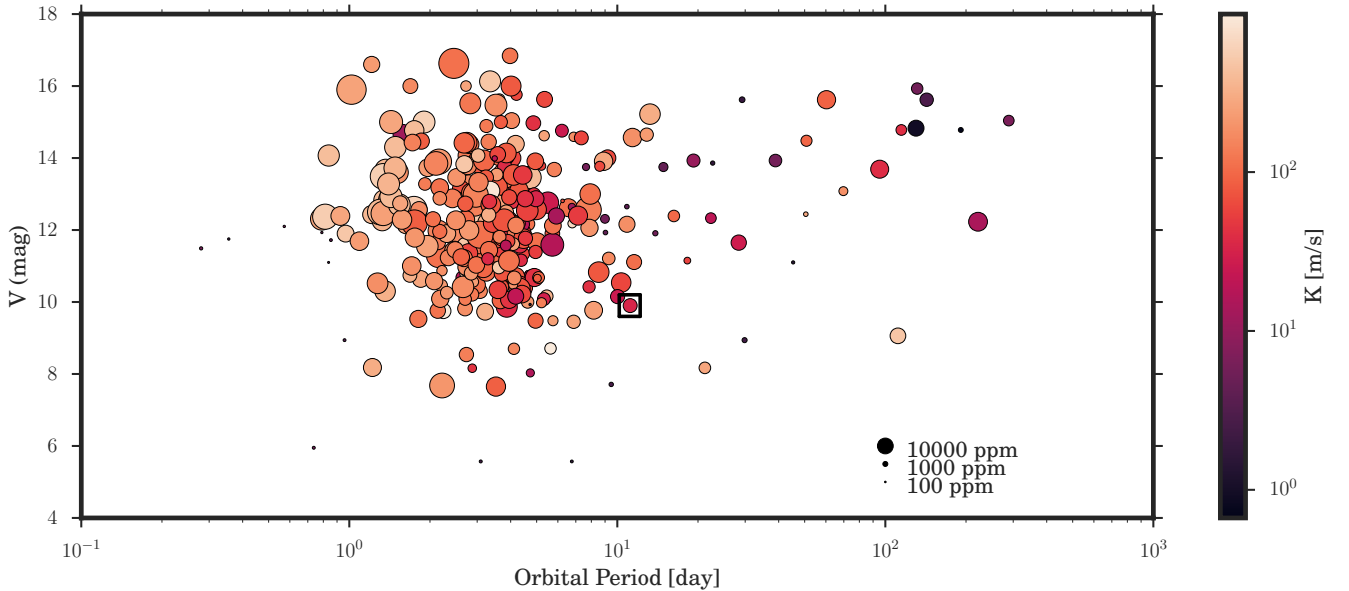


Figure 9. V magnitude as a function of orbital period for the population of transiting planets with masses and radii measured with a precision better than 20%. The size of the points represent the transit depth, while the color is related to the radial velocity semi-amplitude. EPIC247098361b (inside the black square) lies in a sparsely populated region and is one of the few giant planets with $P > 10$ and $V < 10$.

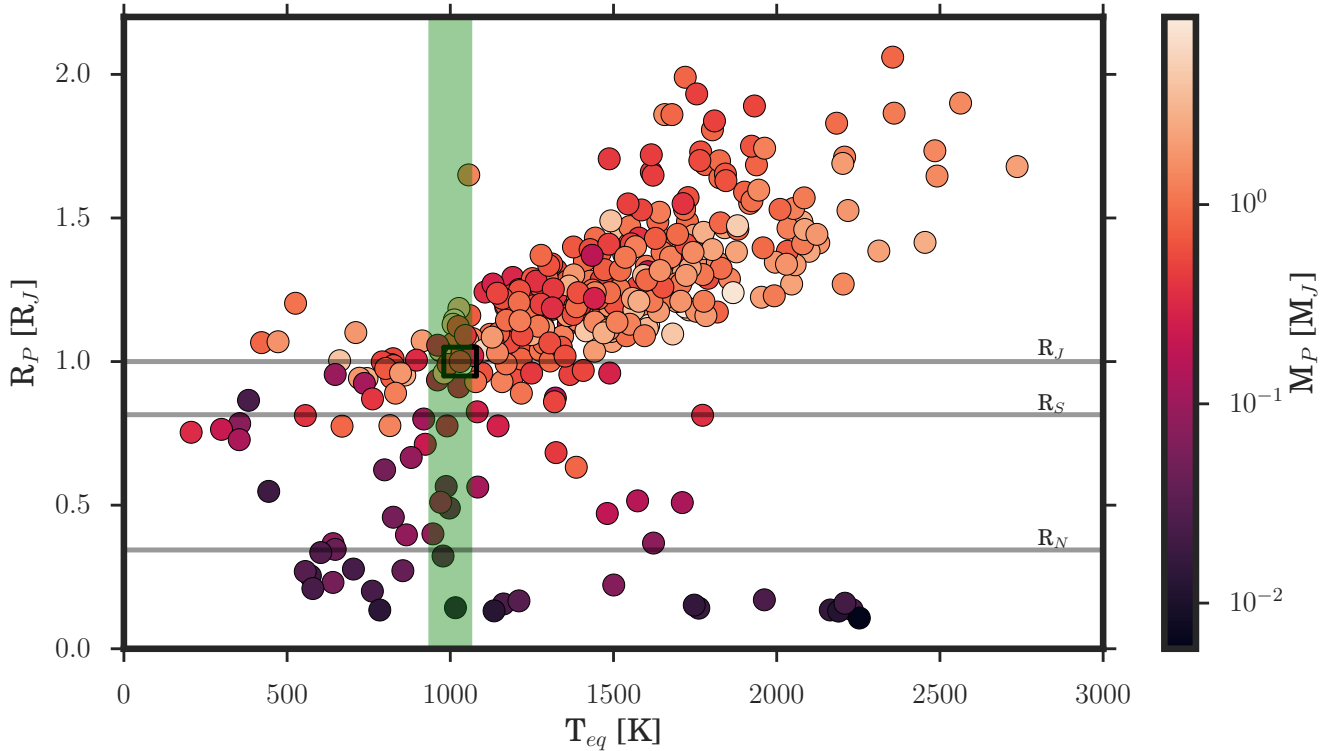


Figure 10. Population of transiting giant planets with radii and masses determined at better than 20% precision level plotted in the T_{eq} - R_* plane. The green vertical bar indicates the transition region for which planets having lower equilibrium temperatures have structures that are not significantly affected by the inflation mechanism of hot Jupiters, EPIC247098361b (inside the black square), lies just inside this transition region.

of the problem but serves as an illustration of the possible internal composition of the planet. We find that, given the evolutionary status of the EPIC247098361 system, the measured mass and radius of the planet are consistent with having a relatively massive central core of $M_{core} = 20 \pm 7 M_{\oplus}$. This value is also consistent with the relation found by Thorngren et al. (2016) between the mass of the planet and the total mass in heavy elements. This relation was obtained using the properties of the known transiting warm giant planets and more realistic models in which the solids are also mixed in an H/He dominated envelope. The prediction for the heavy element mass of EPIC247098361b is $M_Z = 33 \pm 12 M_{\oplus}$, where in this case only $10 M_{\oplus}$ of solids are located in the central core, and a large amount of this material is required to be distributed in the planet envelope to reproduce the observed radius of EPIC247098361b. These properties are consistent with the core accretion model of planet formation (Pollack et al. 1996) in which the planet starts a runaway accretion of gaseous material as soon as the solid embryo reaches a mass of $10 M_{\oplus}$. In this process, the planet keeps accreting rocky and icy planetesimals that have been decoupled from the gaseous disc.

EPIC247098361b is a suitable system on which to use envelope-enriched models to get an independent estimate of M_Z . If put in the context of the full population of transiting warm giant planets, this estimate of M_Z can be used to probe for correlations with other physical and orbital properties. Specifically, Miller & Fortney (2011) found a tentative

correlation between the M_Z and the stellar $[\text{Fe}/\text{H}]$, which then was put in to question by Thorngren et al. (2016) using a bigger sample of systems and new structural models. Nonetheless, the parameters used in the Thorngren et al. (2016) study were not obtained following an homogeneous procedure, and additionally $\approx 25\%$ of their sample consisted of low irradiated systems with orbital periods of $P < 5$ days, whose structure can suffer from other proximity effects (e.g. tidal, magnetic). The combination of GAIA parallaxes, allowing an homogeneous characterization of the host stars, coupled to new discoveries of transiting giant planets with $P > 10$ days by new ground-based (e.g. HATPI¹), and space-based missions (e.g. TESS, Ricker et al. 2014), will be fundamental for linking the inferred heavy element content of the planets with the global properties of the systems.

4.2 Migration

While the current eccentricity of EPIC247098361b is too low to produce significant migration by tidal friction (Jackson et al. 2008), it can still be migrating if the system is being affected by secular gravitational interactions produced by a third distant body (Kozai 1962; Lidov 1962; Li et al. 2014; Petrovich 2015). These interactions produce periodic variations of the eccentricity and inclination of the system, where the interior planet migrates during the very

¹ <https://hatpi.org/>

high eccentricity stage by tidal friction, but most of the time the planet presents moderate eccentricities. Petrovich & Tremaine (2016) presented a model in which only 20% of the warm Jupiter population is migrating through this process. While this conclusion was reached from the eccentricity distribution of radial velocity discovered planets, a stricter test will need a study of the distribution of spin-orbit angles of warm Jupiters. The number of warm Jupiters with measured spin-orbit angles is still low (only 10 studied systems according to TEPcat), and EPIC247098361b is a well suited target for measuring this angle through the Rossiter-McLaughlin effect.

4.3 Possible follow-up observations

The bright host star coupled to the nearly equatorial declination of the system makes of EPIC247098361 one of the most promising warm giant planets to perform detailed follow-up observations using Northern and Southern facilities.

EPIC247098361b is a well suited system to study the atmospheres of moderately low irradiated giant planets. While its expected transmission signal is $\delta_{trans} \approx 450$ ppm, which is small compared to that of typical hot Jupiter systems, there have been reported measurements of transmission spectra for systems with $\delta_{trans} < 500$ and transit depths similar to that of EPIC247098361b. The system is specially interesting for atmospheric studies since it has been predicted that warm Saturns like EPIC247098361b, given its metal enrichment, should have low C/O ratios as compared to that of their host stars (Espinoza et al. 2017b), a picture that has been also predicted for their hotter counterparts from population synthesis models (Mordasini et al. 2016) and thus this might be an excellent system to put this picture to test. In addition, the eccentricity of the system is interesting as different temperature regimes may be at play during transit and secondary eclipse, providing an interesting laboratory for exoplanet atmosphere models.

The EPIC247098361 system is also an ideal target for measuring the spin-orbit angle through the Rossiter-McLaughlin effect. The estimated $v \sin i = 4.2 \text{ km s}^{-1}$ coupled to the planet-star size ratio would produce an anomalous radial velocity signal with a semi-amplitude of $\approx 35 \text{ m s}^{-1}$ for an aligned orbit, which is similar to the orbital semi-amplitude of the system, and which can be measured by numerous spectroscopic facilities.

Warm Jupiters have been proposed to have a significant number of companions in comparison to hot Jupiter systems (Huang et al. 2016). The presence of outer planetary-mass companions is also required for the migration of inner planets through secular gravitational interactions (Dong et al. 2014; Petrovich & Tremaine 2016). EPIC247098361 can be the target of long term radial velocity follow-up observations to detect additional velocity signals or trends that can be associated with distant companions. Finally, EPIC247098361 is a well suited system to search for transit timing variations because its transits can be observed with relatively small aperture telescopes from Southern and Northern facilities.

ACKNOWLEDGMENTS

R.B. gratefully acknowledges support by the Ministry of Economy, Development, and Tourism's Millennium Science Initiative through grant IC120009, awarded to The Millennium Institute of Astrophysics (MAS). A.J. acknowledges support from FONDECYT project 1171208, BASAL CATA PFB-06, and project IC120009 "Millennium Institute of Astrophysics (MAS)" of the Millennium Science Initiative, Chilean Ministry of Economy. A.J. warmly thanks the Max-Planck-Institut für Astronomie for the hospitality during a sabbatical year where part of this work was done. M.R.D. acknowledges support by CONICYT-PFCHA/Doctorado Nacional-21140646, Chile. J.S.J. acknowledges support by FONDECYT project 1161218 and partial support by BASAL CATA PFB-06. This paper includes data collected by the K2 mission. Funding for the K2 mission is provided by the NASA Science Mission Directorate. Based on observations collected at the European Organisation for Astronomical Research in the Southern Hemisphere under ESO programme 0100.C-0487(A).

REFERENCES

- Bakos G., Noyes R. W., Kovács G., Stanké K. Z., Sasselov D. D., Domsa I., 2004, *PASP*, **116**, 266
- Bakos G. Á., et al., 2013, *PASP*, **125**, 154
- Baraffe I., Homeier D., Allard F., Chabrier G., 2015, *A&A*, **577**, A42
- Baranne A., et al., 1996, *A&AS*, **119**, 373
- Barbieri M., et al., 2007, *A&A*, **476**, L13
- Barragán O., et al., 2017, preprint, ([arXiv:1711.02097](https://arxiv.org/abs/1711.02097))
- Borucki W. J., et al., 2010, *Science*, **327**, 977
- Brahm R., et al., 2015, *AJ*, **150**, 33
- Brahm R., et al., 2016a, *PASP*, **128**, 124402
- Brahm R., et al., 2016b, *AJ*, **151**, 89
- Brahm R., Jordán A., Espinoza N., 2017a, *PASP*, **129**, 034002
- Brahm R., Jordán A., Hartman J., Bakos G., 2017b, *MNRAS*, **467**, 971
- Cardelli J. A., Clayton G. C., Mathis J. S., 1989, *ApJ*, **345**, 245
- Coelho P., Barbuy B., Meléndez J., Schiavon R. P., Castilho B. V., 2005, *A&A*, **443**, 735
- Dawson R. I., 2014, *ApJ*, **790**, L31
- Dawson R. I., Johnson J. A., 2018, preprint, ([arXiv:1801.06117](https://arxiv.org/abs/1801.06117))
- Demory B.-O., Seager S., 2011, *ApJS*, **197**, 12
- Dong S., Katz B., Socrates A., 2014, *ApJ*, **781**, L5
- Espinoza N., Jordán A., 2015, *MNRAS*, **450**, 1879
- Espinoza N., Jordán A., 2016, *MNRAS*, **457**, 3573
- Espinoza N., et al., 2016, *ApJ*, **830**, 43
- Espinoza N., et al., 2017a, *MNRAS*, **471**, 4374
- Espinoza N., Fortney J. J., Miguel Y., Thorngren D., Murray-Clay R., 2017b, *ApJ*, **838**, L9
- Foreman-Mackey D., Hogg D. W., Lang D., Goodman J., 2013, *PASP*, **125**, 306
- Fortney J. J., Marley M. S., Barnes J. W., 2007, *ApJ*, **659**, 1661
- Fulton B. J., Petigura E. A., Blunt S., Simukoff E., 2018, preprint, ([arXiv:1801.01947](https://arxiv.org/abs/1801.01947))
- Gaia Collaboration et al., 2016a, *A&A*, **595**, A1
- Gaia Collaboration et al., 2016b, *A&A*, **595**, A2
- Howell S. B., et al., 2014, *PASP*, **126**, 398
- Huang C., Wu Y., Triaud A. H. M. J., 2016, *ApJ*, **825**, 98
- Jackson B., Greenberg R., Barnes R., 2008, *ApJ*, **678**, 1396
- Jones M. I., et al., 2017, preprint, ([arXiv:1707.00779](https://arxiv.org/abs/1707.00779))
- Jordán A., et al., 2014, *AJ*, **148**, 29

- Kaufer A., Stahl O., Tubbesing S., Nørregaard P., Avila G., Francois P., Pasquini L., Pizzella A., 1999, *The Messenger*, **95**, 8
- Kipping D. M., 2013a, *MNRAS*, **435**, 2152
- Kipping D. M., 2013b, *MNRAS*, **435**, 2152
- Kovács G., Zucker S., Mazeh T., 2002, *A&A*, **391**, 369
- Kovács G., et al., 2010, *ApJ*, **724**, 866
- Kozai Y., 1962, *AJ*, **67**, 591
- Kreidberg L., 2015, *PASP*, **127**, 1161
- Lendl M., et al., 2014, *A&A*, **568**, A81
- Li G., Winn J. N., 2016, *ApJ*, **818**, 5
- Li G., Naoz S., Kocsis B., Loeb A., 2014, *ApJ*, **785**, 116
- Lidov M. L., 1962, *Planet. Space Sci.*, **9**, 719
- Luger R., Agol E., Kruse E., Barnes R., Becker A., Foreman-Mackey D., Deming D., 2016, *AJ*, **152**, 100
- Luger R., Kruse E., Foreman-Mackey D., Agol E., Saunders N., 2017, preprint, ([arXiv:1702.05488](https://arxiv.org/abs/1702.05488))
- Mayor M., et al., 2003, *The Messenger*, **114**, 20
- Méndez A., Rivera-Valentín E. G., 2017, *ApJ*, **837**, L1
- Miller N., Fortney J. J., 2011, *ApJ*, **736**, L29
- Mordasini C., van Boekel R., Mollière P., Henning T., Benneke B., 2016, *ApJ*, **832**, 41
- Moutou C., et al., 2009, *A&A*, **498**, L5
- Petrovich C., 2015, *ApJ*, **805**, 75
- Petrovich C., Tremaine S., 2016, *ApJ*, **829**, 132
- Pollacco D. L., et al., 2006, *PASP*, **118**, 1407
- Pollack J. B., Hubickyj O., Bodenheimer P., Lissauer J. J., Podolak M., Greenzweig Y., 1996, *Icarus*, **124**, 62
- Queloz D., et al., 2001, *The Messenger*, **105**, 1
- Rafikov R. R., 2006, *ApJ*, **648**, 666
- Ricker G. R., et al., 2014, in *Space Telescopes and Instrumentation 2014: Optical, Infrared, and Millimeter Wave*. p. 914320 ([arXiv:1406.0151](https://arxiv.org/abs/1406.0151)), doi:10.1117/12.2063489
- Shporer A., et al., 2017, *AJ*, **154**, 188
- Smith A. M. S., et al., 2017, *MNRAS*, **464**, 2708
- Soto M. G., et al., 2018, preprint, ([arXiv:1801.07959](https://arxiv.org/abs/1801.07959))
- Southworth J., 2011, *MNRAS*, **417**, 2166
- Spiegel D. S., Burrows A., 2012, *ApJ*, **745**, 174
- Thorngren D. P., Fortney J. J., Murray-Clay R. A., Lopez E. D., 2016, *ApJ*, **831**, 64
- Winn J. N., Fabrycky D. C., 2015, *ARA&A*, **53**, 409
- Yi S., Demarque P., Kim Y.-C., Lee Y.-W., Ree C. H., Lejeune T., Barnes S., 2001, *ApJS*, **136**, 417
- Zechmeister M., Kürster M., 2009, *A&A*, **496**, 577

Table 4. Radial velocity and bisector span measurements for EPIC247098361.

BJD (-2400000)	RV [km s ⁻¹]	σ_{RV} [km s ⁻¹]	BIS [km s ⁻¹]	σ_{BIS} [km s ⁻¹]	Instrument
58030.8561386	22.4191	0.0103	-0.016	0.012	FEROS
58053.8165988	22.3997	0.0077	0.007	0.010	FEROS
58058.7436015	22.3603	0.0090	0.001	0.011	Coralie
58059.8696367	22.3456	0.0100	-0.041	0.015	Coralie
58060.8694368	22.2747	0.0116	-0.038	0.017	Coralie
58062.8040764	22.3457	0.0072	-0.009	0.009	FEROS
58064.6920866	22.3979	0.0037	0.014	0.005	HARPS
58064.6959210	22.4040	0.0037	0.014	0.005	HARPS
58064.7125895	22.3954	0.0081	-0.013	0.010	FEROS
58065.6785670	22.4072	0.0061	0.006	0.008	HARPS
58065.6823333	22.4117	0.0070	-0.004	0.009	HARPS
58066.7267554	22.4201	0.0053	0.009	0.007	HARPS
58066.7305231	22.4215	0.0050	0.011	0.006	HARPS
58067.7048291	22.4155	0.0053	0.025	0.007	HARPS
58067.7063673	22.4192	0.0061	0.032	0.008	HARPS
58105.6163164	22.3818	0.0162	0.026	0.018	FEROS
58106.7021532	22.3534	0.0071	0.024	0.009	FEROS
58107.6920873	22.3754	0.0070	0.017	0.008	FEROS
58112.6484367	22.4198	0.0070	-0.010	0.008	FEROS
58113.6385671	22.4167	0.0070	0.007	0.007	FEROS
58123.6355085	22.4100	0.0070	0.006	0.008	FEROS
58130.6301555	22.4002	0.0076	0.018	0.010	FEROS
58132.6018895	22.4187	0.0070	0.010	0.008	FEROS
58133.6652444	22.4167	0.0070	0.009	0.009	FEROS
58135.5601350	22.4199	0.0070	0.003	0.009	FEROS
58136.5854351	22.4126	0.0070	-0.001	0.008	FEROS
58140.5838892	22.3587	0.0070	0.002	0.008	FEROS
58141.5782837	22.3755	0.0070	0.005	0.008	FEROS
58142.5699832	22.4076	0.0070	0.010	0.008	FEROS